Macromolecular Bioscience
www.mbs-journal.de

Imidazolium-Based Main-Chain Copolymers With Alternating Sequences for Broad-Spectrum Bactericidal Activity and Eradication of Bacterial Biofilms

Changjiang Liu, Jialei Han, Zeyuan Li, Yadong Liu, Ruodai Wu, Shuaishuai Cao, and Dalin Wu**

In response to the escalating challenge of bacterial drug resistance, the imperative to counteract planktonic cell proliferation and eliminate entrenched biofilms underscores the necessity for cationic polymeric antibacterials. However, limited efficacy and cytotoxicity challenge their practical use. Here, novel imidazolium-based main-chain copolymers with imidazolium (PIm^+) as the cationic component are introduced. By adjusting precursor molecules, hydrophobicity and cationic density of each unit are fine-tuned, resulting in broad-spectrum bactericidal activity against clinically relevant pathogens. PIm^+1 stands out for its potent antibacterial performance, with a minimum inhibitory concentration of 32 μg mL^{-1} against Methicillin-resistant *Staphylococcus aureus* (MRSA), and substantial biofilm reduction in *Staphylococcus aureus* (*S. aureus*) and *Escherichia coli* (*E. coli*) biofilms. The bactericidal mechanism involves disrupting the outer and cytoplasmic membranes, depolarizing the cytoplasmic membrane, and triggering intracellular reactive oxygen species (ROS) generation. Collectively, this study postulates the potential of imidazolium-based main-chain copolymers, systematically tailored in their sequences, to serve as a promising candidate in combatting drug-resistant bacterial infections.

1. Introduction

The global public health crisis of antimicrobial resistance is reaching alarming proportions, particularly in regions where antibiotics are misused.[1,2] To combat this growing problem, antimicrobial peptides (AMPs) have emerged as a promising class of antibacterial agents.[3–5] These peptides, typically consisting of 12–80 amino acid residues, possess an inherent ability to overcome antimicrobial resistance.[6] Characterized by their small size, cationic nature, and amphipathic structures, AMPs effectively interact with and disrupt the membranes of microorganisms, leading to their destruction. Unlike commonly used antibiotics, AMPs exhibit a reduced tendency to induce antimicrobial resistance due to their special mechanism of action, which involves the formation of pores in the microbial membranes, thereby compromising their integrity. Despite demonstrating broad-spectrum activity and rapid antimicrobial efficacy against various microorganisms, the application of AMPs in clinical settings is hindered by challenges such as in vivo hydrolysis, potential toxicity, and high cost.[7–11] In recent decades, research has focused on exploring cationic polymers that can mimic the key features of AMPs; while, offering enhanced proteolytic stability and structural flexibility.[12–14] Consequently, antibacterial polymers have emerged as an increasingly compelling area of investigation. Certain antimicrobial polymers have demonstrated successful applications in areas such as fibers and textiles, self-sterilizing surfaces, medical composites, medical coatings, water filtration systems, antibacterial packaging, and more, yielding satisfactory results.[15–17]

Antibacterial polymers possess cationic moieties and hydrophobic segments in their chemical structure, which plays a crucial role in their sterilizing abilities.[18] These polymers interact with bacterial membranes to achieve sterilization by disrupting the membranes, depolarizing them, or inhibiting membrane synthesis.[19,20] As a result, the development of resistance to antimicrobial polymers is infrequent due to their specific mode of action. The efficacy of antimicrobial polymers relies on their interaction with negatively charged bacterial membranes.[21] The type and density of cations present on the polymers determine the strength of this interaction with microorganisms. Common cations used to impart positive charges to antimicrobial polymers include ammonium,[9,22,23]

C. Liu, J. Han, Z. Li, Y. Liu, D. Wu
Sun Yat-Sen University of Shenzhen Campus
School of Biomedical Engineering
Shenzhen 518107, China
E-mail: wudlin6@mail.sysu.edu.cn
R. Wu, S. Cao
Shenzhen University General Hospital
Shenzhen 518000, China
E-mail: shuaishuai.cao@szu.edu.cn
D. Wu
Guangdong Provincial Key Laboratory of Sensor Technology and Biomedical Instrument
Shenzhen 518107, China
The ORCID identification number(s) for the author(s) of this article can be found under https://doi.org/10.1002/mabi.202300489

DOI: 10.1002/mabi.202300489

sulfonium,[24–26] and phosphonium.[27–29] Among them, antimicrobial polymers containing quaternary ammonium cations have demonstrated notable effectiveness as antiseptics and disinfectants, finding application in products such as mouthwashes and dental materials.[30–33] Moreover, the location of cations along the polymer chain significantly influences their antimicrobial activity. Notably, a comparative study has shown that polymers with cationic species incorporated into the polymer backbone exhibit enhanced antibacterial selectivity and activity compared to their counterparts with cations attached to side chains.[34] More precisely, cationic antimicrobial polymers with amphiphilicity, which are able to mimic the natural structure of AMPs, is an attractive study field.[26,35–37] Very recently, Caihong Lin et al. took advantage of the facially amphiphilic skeletons of bile acids (BAs) and created a main-chain cationic bile acid polymer (MCBAP) with macromolecular facial amphiphilicity via polycondensation and a subsequent quaternization. Their systematic exploration demonstrated that MCBAP with amphiphilic structure displayed an effective activity against Gram-positive methicillin-resistant *Staphylococcus aureus* and Gram-negative *Escherichia coli*, fast killing efficacy, superior bactericidal stability in vitro, and potent anti-infection.[38]

Upon adsorption onto the bacterial membrane surface, antibacterial polymers initiate interactions with microorganisms through their hydrophobic segments, leading to the disruption of membrane integrity. The nature of these hydrophobic segments, including their category, length, and position, has been reported to exert a significant impact on the bactericidal efficiency.[18] Recent studies have clearly demonstrated that antimicrobial polymers containing alternating sequences of hydrophilic and hydrophobic segments exhibit advanced antibacterial effects comparable to natural antimicrobial peptides.[39,40] This similarity to AMPs is likely due to the alternating distribution of blocks in the polymer backbone.[41,42] In addition, the amphiphilic balance of antibacterial polymers significantly influences their ability to achieve pronounced antimicrobial activity against bacteria; while, maintaining satisfactory biocompatibility with mammalian cells.[43,44] Yongjin Hu et al. developed a series of alternating poly-sulfoniums with minimum bactericidal concentrations against Methicillin-resistant *Staphylococcus aureus* (MRSA) and HC_{10} (the lowest polymer concentration that induces > 10% hemolysis of red blood cells [RBC] in the range of 1.25−200 μg mL^{-1} and 4−10 000 μg mL^{-1}), respectively, where the hydrophobicity of each alternating unit can be accurately tuned by altering the monomer precursors.[45]

The interaction of cationic polymers with both bacterial membranes and mammalian cells poses a challenge as it can result in the death or functional impairment of mammalian cells; thus, limiting the clinical application of antibacterial polymers in vivo. Therefore, it is crucial to develop antibacterial polymers that exhibit potent bactericidal activity; while, maintaining moderate biocompatibility.

In natural environments, bacteria predominantly reside within biofilms composed of densely packed extracellular polymeric substances (EPS) consisting of polysaccharides, proteins, lipids, and extracellular DNA.[46,47] Due to the physical insulation provided by EPS, the majority of antibiotics struggle to penetrate and reach the bacteria, resulting in limited antibacterial efficacy.[23,48] Consequently, in order to attain enhanced antibacterial performance, antibacterial polymers need to exhibit not only high bactericidal activity but also efficient disruption of EPS integrity at low concentrations.[26]

Motivated by the growing demands and informative discoveries in the field of antimicrobial polymers, we undertook the design and synthesis of a novel series of antimicrobial polymers (polyimidazolium [PIm^+]) with alternative sequences and variable hydrophobic balances. The PIm^+s were synthesized through condensation polymerization using bi-imidazole and bi-chloride monomers, as depicted in **Scheme 1**. The polymerization process led to the formation of cationic imidazolium groups. Imidazolium cations have been reported to possess enhanced adsorptive capabilities to bacterial cell membranes compared to other quaternary ammonium compounds, attributed to the delocalization of positive charges through the aromatic conjugated imidazole rings.[49] Extensive investigations demonstrated that the antimicrobial activity of the synthesized PIm^+s could be modulated by the nature of the alkyl chains linking the reaction sites of the bi-imidazole and bi-chloride monomers. By adjusting the characteristics of the alkyl linker, a particular antimicrobial polymer (PIm^+1) exhibiting broad-spectrum bactericidal activities against clinically relevant bacteria and a remarkable ability to eradicate biofilms was identified. Further, PIm^+1 exhibited excellent compatibility against red blood cells and negligible potential for inducing antibiotic resistance (15 times bacterial passages), underscoring its significant potential for application in the treatment of chronic bacterial infection-related diseases.

2. Experimental Section

2.1. Materials and Bacterial Strains

Unless otherwise stated, all materials and solvents were used as received. Azobis(isobutyronitrile) (AIBN), 2′,7′-Dichlorofluorescin diacetate (DCFH-DA), and Penicillin–Streptomycin were purchased from Shanghai Sigma–Aldrich Trading Co., Ltd. 1-Vinylimidazole, 1,4-dichlorobutane, 1,6-dichlorohexane, 1,8-dichlorooctane, ethane-1,2-dithiol, butane-1,4-dithiol, hexane-1,6-dithiol, octane-1,8-dithiol, 2,2′-(Ethylenedioxy)diethanethiol, Acetonitrile, and dimethyl sulfoxide (DMSO) were purchased from Shanghai Acmec Biochemical Technology Co., Ltd. Cell Counting Kit-8 (CCK-8), Propidium Iodide Stain Solution (PI), and Hoechst 33342 were purchased from Beijing Labgic Technology Co., Ltd. 3,3′- dipropylthiadicarbocyanine iodide ($DiSC_3[5]$) and *N*-phenyl-1-naphthylamine (NPN) were purchased from Shanghai Macklin Biochemical Technology Co., Ltd. HEPES Buffer Solution was purchased from Suzhou Ant Tao Biotechnology Co., Ltd. Tryptone soybean broth (TSB) powder and agarose were purchased from Guangzhou Huankai microbial Technology Co., Ltd. *E. coli*, ATCC25922; *S. aureus*, ATCC6538; *Pseudomonas aeruginosa* (*P. aeruginosa*, ATCC27853), *Enterococcus faecalis* (*E. faecalis*, ATCC 29212); and MRSA, ATCC43300 were obtained from Shanghai Luwei Technology Co., Ltd.

2.2. Characterization

Proton (^1H) nuclear magnetic resonance (NMR) spectra were recorded on a Bruker NMR system 400 MHz spectrometer

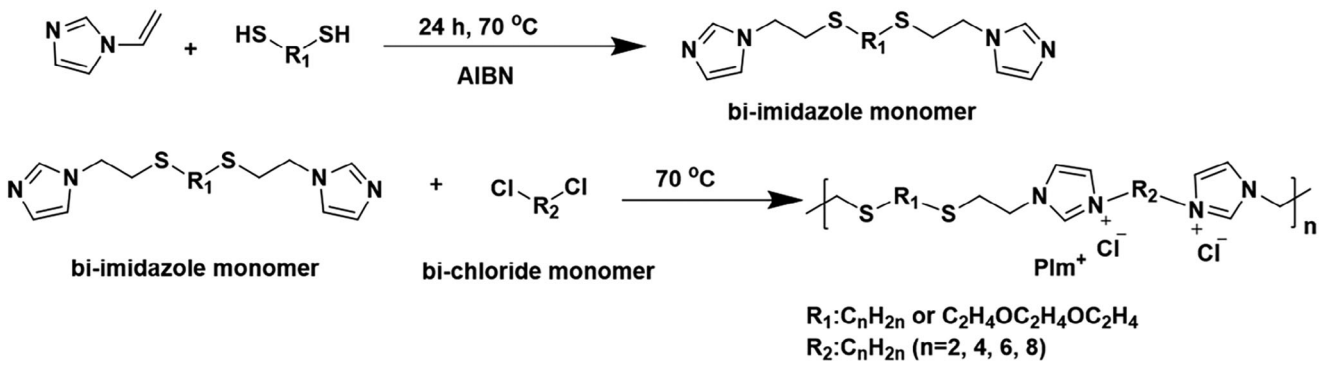

Scheme 1. Detailed synthesis procedure of bi-imidazole monomer and PIm^+.

(Avance III 400 MHz), using $CDCl_3$, DMSO-d_6, and D_2O as the solvents. Scanning electron microscopy (SEM) measurements were performed on a desktop scanning electron microscope (Desktop SEM, Phenom ProX G6). Confocal laser scanning microscopy (CLSM) measurements were imaged on a confocal microscopy system (CLSM, Dragonfly CR-DFLY-202-40). Fluorescence intensity and the optical density were analyzed by flow cytometer (FongCyte Series 3-Laser 14-Color) and microplate reader (synergy H1, BioTek).

2.3. Chemical Structures and Synthetic Protocols of the Compounds

2.3.1. General Synthetic Procedure of Bi-Imidazole Monomer

To a solution of 1-Vinylimidazole (42.5 mmol) and dimercapto monomer (21.25 mmol) in 20 mL dry acetonitrile, was added AIBN (2.125 mmol), and the solution was stirred with an argon bubbler for 15 min. The mixture was stirred at 70 °C overnight, then, concentrated under vacuum to give a crude product. The crude product was purified by flash silica gel column chromatography (v/v = 20:1, dichloromethane-methanol) to give bi-imidazole monomer as a slight yellowish-green oil.

2.3.2. General Synthetic Procedure of PIm+ Polymers

A mixture of di-imidazole monomer, di-chloride monomer, and dry DMSO was stirred for 48 h at 70 °C under argon atmosphere. The reaction mixtures were precipitated into precooled diethyl ether and recrystallized twice in diether ether. The products were dried under a vacuum overnight at room temperature. Following this time, the products were diluted with 15 mL of Milli-Q water and dialyzed (MWCO 3500 g mol^{-1}) for 3 days with regular changes of the solvent. The polymer solution was afterward lyophilized to give a yellow solid.

2.4. The Hydrophobicity Estimation of Alternating Segments

C Log *P* is the Log *P* value obtained by calculation using a medicinal or chemical program. In this study, the hydrophobicities of segment A and segment B in PIm^+ polymers were estimated by *C* Log *P*, which was determined by ChemDraw (version 22.0.0).

2.5. Antibacterial Activity Studies – Minimum Inhibitory Concentration (MIC) Assay and Minimum Bactericidal Concentration (MBC) Assay

Bacteria cells were grown overnight at 37 °C in TSB medium to a mid-log phase and re-suspended in TSB to 2×10^6 colony forming units per mL (CFU mL^{-1}). Polymers were dissolved in PBS buffer (pH = 7.4) at 20 mg mL^{-1}, diluted to different concentrations, and then, mixed 1:1 with bacterial cell suspensions in a 96 well plate. TSB/PBS media (1:1) were inoculated with each strain as a positive control, and TSB/PBS media (1:1) without bacteria inoculum were used as a negative control. All groups were incubated at 37 °C for 24 h, and the optical density of the mixtures at 600 nm (OD_{600}) was measured on a microplate reader. Samples in all experiments were tested in triplicate. MIC was defined as the lowest polymer concentration to inhibit bacterial growth (inhibition% > 90%).

$$\text{Inhibition\%} = \frac{OD_{600}\,(\text{positive control}) - OD_{600}\,(\text{sample})}{OD_{600}\,(\text{positive control}) - OD_{600}\,(\text{negative control})} \times 100\% \quad (1)$$

An aliquot of 5 µL of bacterial suspension from each well of the above final mixture was diluted to 50 µL, transferred to a TSB agar petri dish, and incubated at 37 °C for 24 h. The MBC value was determined as the polymer concentration to achieve > 9 log reduction in the number of viable bacterial cells (CFU) from the control without the polymer. The experiment was repeated at least thrice.

2.6. Hemolysis Assay

The hemolysis reaction was used to analyze the blood compatibility of polymers. The fresh blood was collected from mice and washed repeatedly with PBS buffer (pH = 7.4) to obtain RBC. 200 µL of the RBC suspension was added to PBS solution, achieving desired concentrations of RBC solution in a total volume of 5000 µL. A concentrated solution of polymer was diluted with PBS buffer to different concentrations. Different concentrations of polymers with a constant volume of 500 µL of PBS were added to 500 µL of RBC solution. Each group was designed with three parallel samples, where deionized water and PBS were positive

control and negative control, respectively. The samples were incubated at 37 °C for 2 h, and afterward, the samples were centrifuged to re-pelletize the blood cells. 200 µL of the supernatant of each sample was placed into wells in a 96-well plate, and the optical density at 540 nm (OD_{540}) was measured. The hemolysis rate was calculated by the following equation.

$$\text{Hemolysis\%} = \frac{OD_{540}\,(\text{sample}) - OD_{540}\,(\text{negative control})}{OD_{540}\,(\text{positive control}) - OD_{540}\,(\text{negative control})} \times 100\% \quad (2)$$

2.7. Cytotoxicity Assay

Cell viability kit CCK-8 was used to assess the cytotoxicity of PIm^+ polymers. Mice fibroblast cells (3T3) and human umbilical vein endothelial cells (HUVEC) were seeded into the 96-well cell culture plates at a density of 2000 cells per well. After overnight incubation, the culture medium was aspirated, and 100 µL of a fresh medium containing the polymers to be tested was added into the wells to reach the final concentrations of 8, 16, 32, 64, and 128 µg mL^{-1}. After 24 h, the medium was removed and the cells were washed with sterile PBS. Then, 100 µL of fresh medium containing CCK-8 was added to each well. The plate was further incubated at 37 °C for 4 h. Optical density at 450 nm (OD_{450}) was recorded using the microplate reader.

2.8. Outer Membrane (OM) Permeabilization

NPN was used as the fluorescent probe to characterize the outer membrane permeabilization of *E. coli*.[50] Bacteria were cultured to the mid-log phase (OD_{600} = 0.6). After centrifugation (4000 rpm, 3 min, 4 °C), the supernatant was decanted, and the pellet was resuspended in 5 mL of the HGK buffer solution (a buffer solution containing 5 mM HEPES, 20 mM glucose, and 20 mM KCl, pH 7.4) to obtain the bacterial working suspension (≈10^9 CFU mL^{-1}). Next, 50 µL of the NPN solution (40 µM) was pipetted into each well of a 96-well plate containing 100 µL of the bacterial working suspension. The fluorescence intensity was monitored at excitation and emission wavelengths of 350 and 420 nm, respectively. When the readings of fluorescence intensity were stable, a 50 µL aliquot of the HGK buffer solution (pH 7.4) containing antibacterial agent was added; following which (time = 0 min), the fluorescence intensity was recorded continuously.

2.9. Cytoplasmic Membrane (CM) Permeabilization Assay

The cytoplasmic membrane permeabilization was characterized by using PI uptake assay, and the fluorescent intensities were recorded at λ_{ex} = 535 nm and λ_{em} = 617 nm. The other procedures were the same as the OM permeabilization assay, except that the final concentration of PI was 10 µM, and the final concentrations of polymers were at 16 µg mL^{-1} (MBC for *E. coli*), 32 µg mL^{-1} (2× MBC for *E. coli*), 64 µg mL^{-1} (MBC for *S. aureus*), and 128 µg mL^{-1} (2× MBC for *S. aureus*), respectively.

2.10. Cytoplasmic Membrane Depolarization Assay

The depolarization of CM was characterized by using $DiSC_3(5)$ as the fluorescent probe. 96-well plate containing 100 µL bacterial working suspension was prepared. For *E. coli*, an extra 0.33 mM of EDTA was added into the working suspension. After incubating for 20 min at 37 °C, 30 µL of $DiSC_3(5)$ was added to reach a final concentration of 4 µM. The fluorescence intensities were recorded using a microplate reader at λ_{ex} = 622 nm and λ_{em} = 670 nm. When the fluorescence intensity became stable, a 50 µL aliquot of the HGK buffer solution (pH 7.4) containing each antibacterial agent was pipetted into each well (time = 0 min) to achieve a final concentration at 16 µg mL^{-1} (MBC for *E. coli*), 32 µg mL^{-1} (2× MBC for *E. coli*), 64 µg mL^{-1} (MBC for *S. aureus*), or 128 µg mL^{-1} (2× MBC for *S. aureus*), and the fluorescent intensity of each well was recorded continuously.

2.11. Intracellular ROS Generation

DCFH-DA was applied to determine the level of intracellular ROS. In brief, each bacteria was incubated with Plm^+1 at twice the concentration of MBC for 1 h at 37 °C. Subsequently, the suspension was stained by DCFH-DA (25 µM) before centrifuging and washed with PBS. At last, the fluorescence of DCFH was utilized by flow cytometry.

2.12. Bacterial Morphology Measurement

The morphologies of *S. aureus* and *E. coli* treated with or without polymers were examined using SEM operated at 3 kV. In general, polymer was added to the 1 mL bacterial suspension of *S. aureus* and *E. coli* (10^7 CFU mL^{-1}) to reach a final concentration of 16 and 64 µg mL^{-1}, respectively. Bacterial suspension without any polymer was used as the control. After incubation at 37 °C for 2 h, all samples were fixed in the glutaraldehyde solution (pH 7.2, 2.5%) for 12 h at room temperature. The bacterial cells were dehydrated using gradient ethanol solutions (20%, 50%, 70%, 80%, 90%, and 100% v/v in water) and dried in air on a silicon slice, then, coated with gold for 60 s and observed by SEM.

2.13. CLSM Imaging of Polymer-Treated Bacteria

To observe the colocalization of polymers with bacteria, exponentially growing bacteria were collected by centrifugation at 4000 rpm for 5 min, washed with PBS, and diluted. The bacterial suspensions were then incubated with 128 µg mL^{-1} polymer for 4 h, followed by staining with Hoechst 33342 and PI. Fluorescent images were taken from the confocal laser scanning microscope.

2.14. Biofilm Eradication Assay

Exponentially growing bacteria were inoculated in a 96-well plate (1×10^6 cells per well) containing TSB and incubated under stationary conditions at 37 °C for 2 days. After biofilm formation, the medium was discarded, and the plates were washed with PBS to

remove the planktonic bacteria. Fresh TSB containing serially diluted polymer was added to the plates and incubated at 37 °C for another 12 h. Finally, the biofilm biomass was quantified by the crystal violet staining method.

2.15. CLSM Observations of the Polymer Penetration to Biofilms

S. aureus and *E. coli* biofilms were grown in a glass-bottom Petri dish for 2 days. The biofilms were incubated with polymer for 30, 60, 90, and 120 min, followed by the staining with Hoechst 33342. The biofilm was then washed with PBS twice and monitored by CLSM.

2.16. 3D CLSM Live/Dead Staining Images of Mature Biofilms

S. aureus and *E. coli* biofilms were grown in a glass-bottom Petri dish for 2 days. The biofilms were incubated with polymer for 12 h, followed by the staining with Hoechst 33342 and PI. The biofilm was then washed with PBS twice and monitored by CLSM.

2.17. Bacterial Killing Kinetics Study

The *S. aureus* and *E. coli* bacteria strains were inoculated and prepared by a similar procedure used for MIC determination studies. The suspensions of *S. aureus* and *E. coli* (2×10^6 CFU mL^{-1}) in PBS were prepared, followed by the addition of the PIm^+ polymer at 2× MBC. At different incubation times (1, 5, 10, 15, 30, 60, and 120 min), the mixture was sampled and dropped onto the TSB agar plates and spread evenly. The plates were then incubated at 37 °C for 24 h to examine the colony numbers for survival counting and viability calculation using ImageJ program.

2.18. Drug Resistance Study

The first MIC determination of PIm^+ polymer was performed as described above. Bacterial samples from triplicate wells (60 µL) at 1/2 of MIC (16 µg mL^{-1} for *S. aureus* and 4 µg mL^{-1} for *E. coli*) were removed and added to fresh TSB medium (1.5 mL). The bacterial culture was regrown at 37 °C to reach the mid log growth phase. MIC values of PIm^+ polymers were determined following the similar procedure as described above. Drug resistance experiments were performed on *S. aureus* and *E. coli* by repeated treatment with PIm^+ polymer for 15 passages. The groups treated with Penicillin–Streptomycin were used as controls.

2.19. Stability Evaluation of PIm^+1 Polymers

D_2O was used as a solvent to prepare the PBS buffer for the stability study. A 550 µL solution of 10 mg PIm^+1 polymer was prepared in D_2O in an NMR tube. ^{1}H-NMR spectra were recorded after the solution was stored for 0 day, 1 month, and 3 months at 37 °C, as well as after heating to 80 °C for 18 h.

2.20. Statistical Analysis

Software GraphPad Prism 9.5 was used for statistical analysis. The CCK-8 data were evaluated by one-way analysis of variance (ANOVA), and overall differences were considered significant at the 5% level. The unpaired double-tailed *t*-test was used to calculate the significant difference (*p* value) between groups for biofilm mass data. $p < 0.05$ was considered to demonstrate statistically significant differences. The significance level was indicated as * < 0.05, ** < 0.01, *** < 0.001, and **** < 0.0001.

3. Results and Discussion

3.1. Synthesis and Characterization of Polyimidazolium (PIm^+)

In this study, a series of PIm^+ copolymers with an alternating repeating unit sequence was synthesized through 2 + 2 condensation polymerization using equimolar ratios of bi-imidazole monomers (Im-R1-Im (R1: C_nH_{2n} [n = 2, 4, 6, 8] or $C_2H_4OC_2H_4OC_2H_4$)) and bi-chloride monomers (Cl-R2-Cl (R2: C_nH_{2n} [n = 2, 4, 6, 8]). The synthesis procedure and structural elucidation of the bi-imidazole monomers and PIm^+ copolymers are illustrated in Scheme 1. Bi-imidazole monomers were prepared via a highly efficient thiol-ene click reaction between 1-vinylimidazole and a bi-thiol compound, employing AIBN as the initiator. The detailed experimental procedure and conditions can be found in the Experimental Section. The high purity of the bi-imidazole monomers is evident from the clean ^{1}H NMR spectra (see Figure S1, Supporting Information), ensuring the success of the subsequent 2 + 2 condensation polymerization. For PIm^+s copolymer synthesis, the polymerization process relied on the quaternization reaction between the imidazole groups and alkyl chlorides. The successful quaternization and polymerization were confirmed by ^{1}H NMR spectrum (**Figure 1**). In detail, the chemical shift values of the protons in the imidazole group changed from ≈6.95–7.05 ppm (g, Figure 1A) to ≈7.44–7.50 ppm (g, Figure 1B) during the polymerization. The stoichiometric ration between monomers and polymerization duration was carefully controlled to regulate the viscosity of the polymerization medium and the molecular weight of the resulting PIm^+ polymers. It is important to note that although the bi-imidazole monomers contained a thioether moiety capable of alkylation reactions in the presence of alkyl chlorides, the presence of alkene proton resonances (next to the sulfur atom) at $\delta = 2.95$ and $\delta = 2.48$ in the ^{1}H NMR spectrum of PIm^+ copolymers (Figure S2, Supporting Information), without any changes in integral areas and chemical shift, confirmed that the quaternization occurred exclusively between the imidazole and alkyl chloride groups. This observation supports the notion that if alkylation was to occur at the sulfur atoms, the alkene protons adjacent to the sulfur atoms would shift to a lower field due to the stronger electronegativity of sulfonium.[26]

Certain studies have suggested that the number average molecular weight ($\overline{M_n}$) and polydispersity index (PDI) of antibacterial polymers may impact their bactericidal performance. However, the determination of $\overline{M_n}$ and PDI for PIm^+ copolymers using gel permeation chromatography (GPC) was not feasible due to the high density of cationic charges present on their

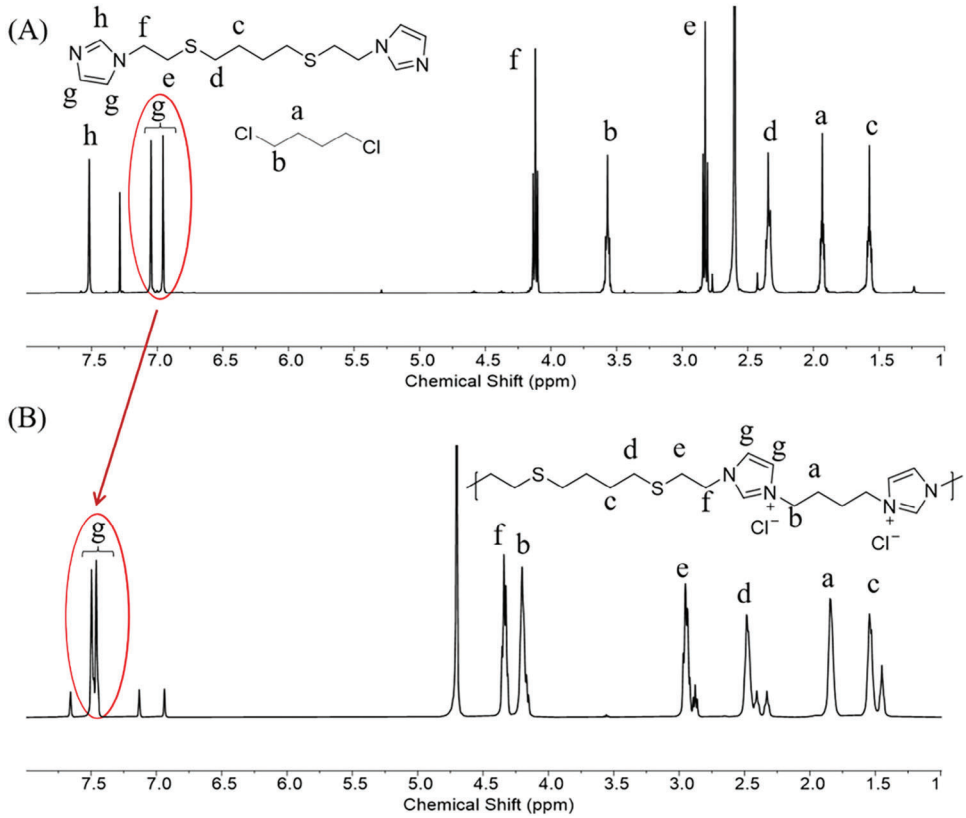

Figure 1. The comparison of ^{1}H NMR spectrums of polymerization medium A) before and B) after polymerization. The proton on the imidazole group was highlighted with red ellipses.

backbones. Therefore, the $\overline{M_n}$ of PIm$^+$ polymers was calculated using Equations (3) (Carothers equation)[51] and (4):

$$\bar{X}_n = \frac{1}{1-p} \tag{3}$$

$$\overline{M_n} = \overline{X_n}\, M_0 \tag{4}$$

where p is the degree of reaction of the groups and M_0 is the average molecular weight of the structural unit. p was achieved by calculating one minus the ratio of the integral area of protons on imidazole end group to the integral area of protons on imidazolium of the polymerization medium according to ^{1}H NMR spectrum. It is reported that a molecular weight ranging from 6000 to 50 000 g mol^{-1} has no obvious trend of antibacterial activity and biocompatibility linked to the changing of polymer chain length.[52] In this exploration, 15 PIm$^+$s with $\overline{M_n}$ ranging from 0.6 to 2.1 kDa were prepared. The detailed chemical structure information of them is displayed in **Table 1**. The corresponding ^{1}H NMR spectrums of PIm$^+$s are presented in Figures S3–S7, Supporting Information.

The incorporation of quaternary ammonium salts in the PIm$^+$s imparts them with hydrophilicity and enables PIm$^+$s to interact with microbial membranes. In addition, the hydrophobicity of the PIm$^+$s can be readily adjusted by utilizing monomers with different alkylene linkers. The synthesis of PIm$^+$s through condensation polymerization ensures that the hydrophilic and hydrophobic units are arranged in an alternating sequence manner within the polymer backbone. For ease of discussion, the repeating units of the PIm$^+$s are divided into two segments: segment A deriving from bi-imidazole monomers and segment B originating from bi-chloride monomers, as illustrated in Table 1.

3.2. Planktonic Microbe Antibacterial Activity and Hemolytic Toxicity

To preliminarily investigate the antibacterial activity of PIm$^+$s, three variants (PIm$^+$1, PIm$^+$2, and PIm$^+$3) differing in amphiphilicity were synthesized using a fixed bi-imidazole monomer (R_1: C_4H_8) and three distinct bi-chloride monomers (R_2: C_4H_8, C_6H_{12}, C_8H_{16}) (see Table 1). The ^{1}H NMR spectra of these polymers are provided in Figure S3, Supporting Information. To mitigate the impact of $\overline{M_n}$ on the biological performance, the $\overline{M_n}$ values of the aforementioned three PIm$^+$s were controlled within the range of 0.6 to 1.1 kDa (Table 1). Subsequently, the antibacterial activity and hemolytic toxicity of the three PIm$^+$ variants were evaluated against MRSA, which is one of the resistant clinical strains, and RBC. Remarkably, all three PIm$^+$s exhibited an identical minimal MBC of 32 μg mL^{-1} against MRSA (**Figure 2A**); while, the MIC for the three PIm$^+$ variants ranged from 16 μg mL^{-1} (PIm$^+$3) to 32 μg mL^{-1} (PIm$^+$1 and PIm$^+$2). These results indicate that the length of the hydrophobic linker in the bi-chloride monomers among

Table 1. Detailed chemical structure and $\overline{M_n}$ of PIm$^+$s.

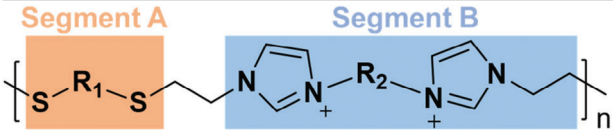

Polymers[a)]	R_1	R_2	$\overline{M_n}$	Polymers	R_1	R_2	$\overline{M_n}$
PIm$^+$1	C_4H_8	C_4H_8	6100	PIm$^+$9	C_6H_{12}	C_8H_{16}	12 900
PIm$^+$2	C_4H_8	C_6H_{12}	8300	PIm$^+$10	C_8H_{16}	C_4H_8	13 500
PIm$^+$3	C_4H_8	C_8H_{16}	11 400	PIm$^+$11	C_8H_{16}	C_6H_{12}	19 100
PIm$^+$4	C_2H_4	C_4H_8	8800	PIm$^+$12	C_8H_{16}	C_8H_{16}	21 600
PIm$^+$5	C_2H_4	C_6H_{12}	15 100	PIm$^+$13	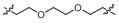	C_4H_8	7600
PIm$^+$6	C_2H_4	C_8H_{16}	14 300	PIm$^+$14	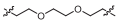	C_6H_{12}	9000
PIm$^+$7	C_6H_{12}	C_4H_8	9200	PIm$^+$15	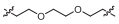	C_8H_{16}	10 300
PIm$^+$8	C_6H_{12}	C_6H_{12}	9700	—	—	—	—

[a)] Structures of segments A and B are marked in orange and blue, respectively.

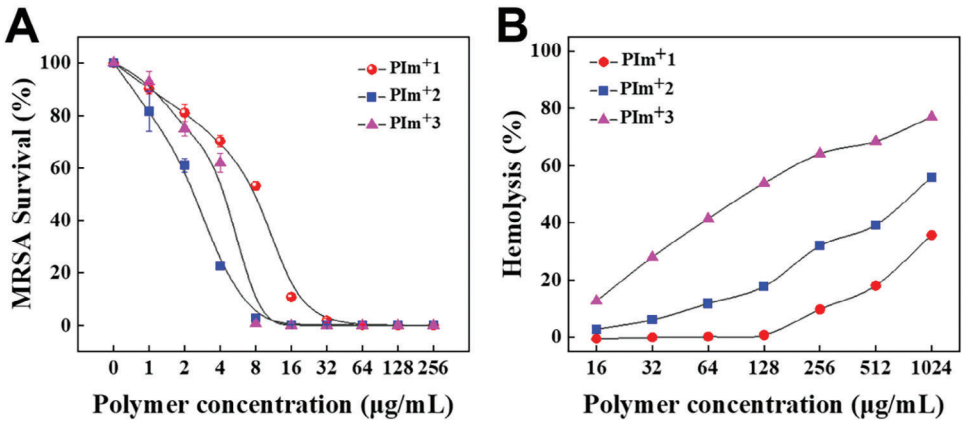

Figure 2. A) Viability of MRSA and B) percentage hemolytic of RBC induced by PIm$^+$1, PIm$^+$2, and PIm$^+$3 copolymers at different concentrations.

these three polymers has negligible influence on the MIC and MBC. Further, the observed MBC values equaling the MIC values suggest that the above-mentioned antibacterial polymers acted as effective bactericidal agents rather than solely inhibiting microbial growth. In contrast, their hemolytic activities strongly correlated with the length of the hydrophobic linker in the bi-chloride monomers (Figure 2B). PIm$^+$2 (HC_{10} = 32 μg mL^{-1}) and PIm$^+$3 (HC_{10} < 16 μg mL^{-1}) exhibited significant hemolytic toxicity; while, PIm$^+$1 demonstrated excellent biocompatibility against mammalian cells, as indicated by its HC_{10} value of 256 μg mL^{-1}, which was eight times higher than that of PIm$^+$2 and 16 times higher than that of PIm$^+$3. To systematically evaluate the antibacterial activity of the three PIm$^+$ variants, their MBC and MIC values were determined against other non-bactericidal-resistant Gram-positive bacteria (*S. aureus* and *E. faecalis*) and Gram-negative bacteria (*E. coli* and *P. aeruginosa*). As shown in **Table 2**, similar to their activity against MRSA, all three PIm$^+$s exhibited comparable antibacterial activity (MBC = 8–64 μg mL^{-1}, MIC = 8–64 μg mL$_{-1}$) against *S. aureus, E. faecalis, E. coli*, and *P. aeruginosa*. Notably, the PIm$^+$ variants demonstrated superior antibacterial activity against *E. coli* (MBC = 8 μg mL^{-1}, MIC = 64 μg mL^{-1}) compared to other bacteria. These findings underscore the significant impact of the chemical structures of PIm$^+$s on their bactericidal activity and hemolytic performance.

To thoroughly investigate the influence of the chemical structures of PIm$^+$s on their antibacterial performance and hemocompatibility, another series of PIm$^+$ variants (PIm$^+$4–PIm$^+$12) with varying hydrophobicity was synthesized using different bifunctional monomers with variable lengths of linkers between reaction sites (Table 1). The chemical structures of PIm$^+$4–PIm$^+$12 were confirmed through ^{1}H NMR analysis (Figures S4–S6, Supporting Information). The hydrophobicity level, which significantly affects the antibacterial activity of polymers, is often described using the *C* Log *P* values. In our study, the *C* Log *P* values for segment A ranged from 2.35 to 5.22; while, for segment B, they ranged from 2.81 to 4.93 (Table S1, Supporting Information). For the convenience of comparison, we calculated the *C* Log *P* values of the different segments in molecules, such as alkane chains, without calculating the same parts, such as sulfur atoms and imidazole groups. A higher *C* Log *P* value indicates a greater degree of hydrophobicity. The antibacterial activity and hemolysis behavior of PIm$^+$4–PIm$^+$12

Table 2. Characterization and biological performances of PIm^+s.

Polymers	MRSA[a]		*S. aureus*[b]		*E. faecalis*[c]		*E. coli*[d]		*P. aeruginosa*[e]			
	MIC [μg mL^{-1}]	MBC [μg mL^{-1}]	MIC [μg mL^{-1}]	MBC [μg mL^{-1}]	MIC [μg mL^{-1}]	MBC [μg mL^{-1}]	MIC [μg mL^{-1}]	MBC [μg mL^{-1}]	MIC [μg mL^{-1}]	MBC [μg mL^{-1}]	HC_{10}[f] [μg mL^{-1}]	HC_{50}[g] [μg mL^{-1}]
PIm^+1	32	32	32	64	64	64	8	16	32	32	256	>1024
PIm^+2	32	32	64	64	64	64	8	8	64	64	32	512
PIm^+3	16	32	16	32	32	64	8	8	16	16	<16	32
PIm^+4	>256	>256	256	256	128	128	32	32	128	128	512	>1024
PIm^+5	256	256	256	256	256	256	16	32	32	32	16	128
PIm^+6	256	256	256	>256	256	256	16	16	32	64	<16	128
PIm^+7	32	32	32	32	128	256	8	16	32	32	<16	64
PIm^+8	16	32	16	16	16	16	16	16	16	16	<16	32
PIm^+9	8	8	8	16	4	4	16	16	4	4	<16	16
PIm^+10	128	128	64	128	64	64	32	64	16	32	<16	<16
PIm^+11	32	64	8	8	16	16	32	32	32	64	<16	<16
PIm^+12	8	8	8	8	8	16	32	32	16	32	<16	<16
PIm^+13	>256	>256	>256	>256	>256	>256	256	256	256	256	>1024	>1024
PIm^+14	>256	>256	256	>256	>256	>256	256	256	>256	>256	>1024	>1024
PIm^+15	64	64	32	32	32	32	128	128	16	16	>1024	>1024

[a] MRSA: Methicillin-resistant *Staphylococcus aureus*, ATCC43300; [b] *S. aureus: Staphylococcus aureus*, ATCC6538; [c] *E. faecalis: Enterococcus faecalis*, ATCC29212; [d] *E. coli: Escherichia coli*, ATCC25922; [e] *P. aeruginosa: Pseudomonas aeruginosa*, ATCC27853; [f] HC_{10}: the lowest polymer concentration that induces > 10% hemolysis of RBC; [g] HC_{50}: the lowest polymer concentration that induces > 50% hemolysis of RBC.

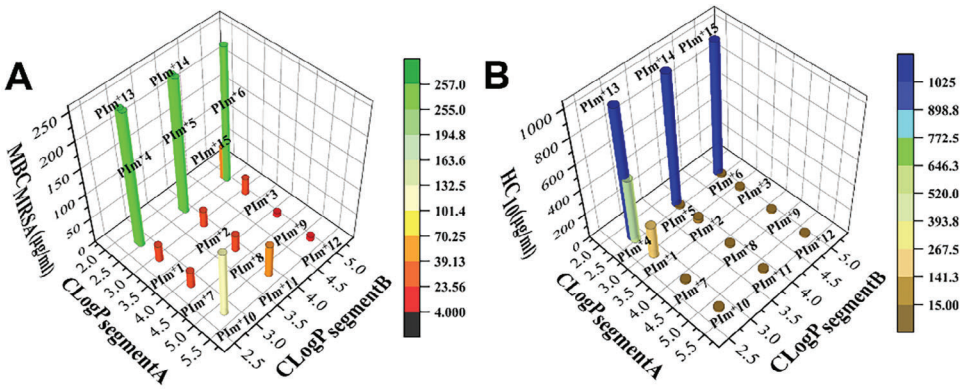

Figure 3. Diagram of the antibacterial activity and hemolysis performances of PIm^+s. A) Minimum bactericidal concentrations (MBCs, the lowest polymer concentration that achieved ≥ ninefold log reduction in the number of viable bacterial cells) against MRSA and B) HC_{10} (the lowest polymer concentration that induces > 10% hemolysis of RBC) with different hydrophobicity of the segments in PIm^+ polymers. *C* Log *P* represents the calculated hydrophobic values of each segment.

were evaluated against the aforementioned bacteria and RBC as well, and the results are presented in **Figure 3** and Table 2. According to Figure 3A, PIm^+ variants (PIm^+1, PIm^+2, PIm^+3, PIm^+7, PIm^+8, PIm^+9, and PIm^+12) exhibited superior antibacterial activity against MRSA (MBC = 8–32 μg mL^{-1}). Regarding hemocompatibility, only PIm^+1 (HC_{10} = 256 μg mL^{-1}) and PIm^+4 (HC_{10} = 512 μg mL^{-1}) exhibited excellent biocompatibility. Among all of the PIm+ variants, PIm^+1 holds moderate *C* Log *P* values (segment A = 3.11 and segment B = 2.81), more excellent antibacterial efficacy, and greater biocompatibility than other PIm^+ variants. Overall, the presence of longer hydrophobic linkers in the bi-imidazole monomers (higher *C* Log *P* value) enhanced antibacterial activity; while, reducing hemolytic compatibility of PIm^+s, which aligns with previously reported cases. Yongjin Hu et al. detailed an obvious trend that the bactericidal efficiency of polymers was enhanced with the increase of *C* Log *P* values in segments combined with higher toxicity, which shows that the structural composition and hydrophobicity of alternating antibacterials is essential for optimization of antimicrobial activity and low toxicity.[45] In addition, similar to PIm^+1–PIm^+3, PIm^+4–PIm^+6 also exhibited enhanced antibacterial efficacy against *E. coli* compared to other bacterial strains (Table 2).

Not only alkyl chains with different lengths were introduced to investigate the influence of chemical structures on antibacterial performances but also the PEG with stronger hydrophilicity compared with alkyl chains was introduced to fabricate the antibac-

terial polymers. In total, three new antibacterial polymers with PEG as the segment A were synthesized and named as PIm^+13, PIm^+14, and PIm^+15. The chemical structures of them together with ^1H NMR spectrums are present in Figure S7, Supporting Information. According to the values of MIC, MBC, and HC_{10} against various bacteria (Table 2), the introduced PEG indeed influenced the antibacterial and biocompatibility performances. For example, compared with PIm^+1 and PIm^+13, which held the same segment B (C_4H_8) and the relatively same molecular weight (6100–7600), PIm^+1 (MIC = 8–64 μg mL^{-1} and MBC = 16–64 μg mL^{-1}) held better antibacterial efficacy than PIm^+13 (MIC > 256 μg mL^{-1}, MBC > 256 μg mL^{-1}). Taking PIm^+3 and PIm^+15 as another typical comparison, which held the same segment B (C_8H_{16}) and the relatively same molecular weight (10 300–11 400), obviously, PIm^+15 (HC_{10} > 1024 μg mL^{-1}) held more excellent biocompatibility than PIm^+3 (HC_{10} < 16 μg mL^{-1}), which is attributed to the great biocompatibility of PEG in PIm^+15.

After careful evaluation of the antibacterial activities and hemolytic performances of all PIm^+ variants, it was observed that PIm^+1, PIm^+2, and PIm^+15 exhibited both high-performance antibacterial profiles against microbes and excellent biocompatibility with RBC. For antibacterial polymers, selectivity which is calculated as HC_{10}/MBC, is often considered as a critical parameter to evaluate the safety.[26] The values of selectivity of PIm^+1, PIm^+2, and PIm^+15 against MRAS are 8, 1, and 16, respectively. Considering that alkyl chain-based antibacterial polymer is the main investigating objective in our original design, only PIm^+1 was selected for in-depth mechanism studies on biofilm eradiation in this report. To comprehensively assess its biocompatibility, PIm^+1 was also co-cultured with 3T3 and HUVEC, allowing the evaluation of cytotoxicity. Encouragingly, all cell lines exhibited over 80% cell viability up to 128 μg mL^{-1} (Figure S8, Supporting Information), indicating the selective biocompatibility of PIm^+1 toward mammalian cells.

3.3. Bactericidal Mechanism Exploration

Antibacterial polymers typically achieve their bactericidal effects through the adsorption of cationic moieties onto the negative phosphate groups of bacterial cell membranes via electrostatic interactions, as well as the release of cytoplasmic components resulting from the insertion of hydrophobic segments into the membrane.[19] Clearly, these processes of cell membrane damage play a crucial role in determining the antibacterial performance of antibacterial polymers and warrant further investigation in depth. The schematic illustration of the action mechanisms of PIm^+ against *E. coli* and *S. aureus* is shown in **Figure** 4A. To assess membrane permeabilization and cytoplasmic membrane depolarization, experiments were conducted using PIm^+1 against *E. coli*, MRSA, and *S. aureus*. Upon addition of PIm^+1 solution (2× MBC) to *E. coli*, an increase in fluorescence intensity of NPN was observed (Figure 4B), indicating that the permeabilization of the outer membrane of Gram-negative bacteria happened. For evaluating cytoplasmic membrane permeabilization and depolarization, we employed DiSC3(5) as a fluorescence indicator. DiSC3(5) experiences self-quenching of fluorescence upon reaching high concentrations in the cytoplasmic membrane. As the membrane potential dissipates thereafter, fluorescence is restored, facilitating the assessment of membrane permeabilization and depolarization.[45] The rapid increase in fluorescence intensity from $DiSC_3(5)$ within the first 10 min following treatment with PIm^+1 (MBC and 2× MBC) suggests the occurrence of cytoplasmic membrane depolarization resulting from the electrostatic absorption of PIm^+1 (Figure 4C–E). In addition, we continued to investigate the capability of PIm^+1 to disrupt the CM integrity by the notable increase in fluorescence intensity of PI (Figure 4F–H), a fluorescent probe that could enter CM-compromised bacterial cells and specifically emit fluorescence upon binding with DNA, upon treatment of bacteria with PIm^+1 (at MBC and 2× MBC concentrations). It has been reported that antibacterial cationic polymers could induce the overgeneration of ROS in bacteria. Interestingly, PIm^+1 selectively triggered a significant increase in ROS production in the Gram-negative bacterium *E. coli* (Figure 4I), which aligned with findings by Anzhi Wang et al. using fluoroalkylated polyethylenimines (PEI-F) as antibacterial polymers.[50] However, the Gram-positive bacteria MRSA and *S. aureus* did not exhibit a similar response to PIm^+1, in terms of ROS overproduction (Figure 4I). The underlying reasons for this differential response, where only *E. coli* generates extra ROS in the presence of antibacterial cationic polymers while MRSA and *S. aureus* do not, remains unknown and requires further investigation.

Based on these findings, the live/dead fluorescence assay using CLSM revealed a perfect overlay of blue signal (Hoechst 33342 signal for bacteria), green signal (autofluorescence signal for PIm^+1), and red signal (PI signal for released DNA), indicating the excellent affinity of PIm^+1 toward both *S. aureus* and *E. coli* (Figure S9, Supporting Information). To further investigate the impact of PIm^+1 on bacterial membrane integrity, the surface morphology of *E. coli* and *S. aureus* was examined using SEM after a 2-h exposure to PIm^+1 (at 2× MBC concentration). In comparison to the control group, which exhibited intact membrane integrity in the absence of PIm^+1 treatment, the presence of PIm^+1 caused noticeable disruptions in the membranes of both *E. coli* and *S. aureus* (**Figure** 5A). These observations directly demonstrate that the antibacterial mechanism of PIm^+1 against bacterioplankton is analogous to that of AMPs as it involves the disruption of the bacterial membrane.[50] The antibacterial performance of PIm^+1 against *S. aureus* and *E. coli* was also evaluated by monitoring the number of viable bacterial colonies at specific time intervals, as shown in Figure 5B. For *S. aureus*, killing efficiencies of at least 3 log reduction (>99.9%) in colony counts at MBC value were achieved at 1 h; while, the time needed to achieve at least a 3 log reduction for *E. coli* was reduced to 30 min at MBC. These results provide strong evidence that PIm^+1 is bactericidal rather than simply inhibiting the growth of the microbes.

The types of counter ions in antibacterial polymers hold influence on their antibacterial performance.[53,54] For our PIm^+ variants, chloride ions acted as the counter ions. It was reported that the antimicrobial ability chloride ions showed negligible effect on the antimicrobial activity of polymers.[55,56]

Our investigations have demonstrated that PIm^+1 exhibits the ability to interact with the bacterial membrane, with its hydrophobic segments capable of penetrating the membrane and compromising its integrity. However, in real-world scenarios, bacteria primarily reside within robust biofilms. Therefore,

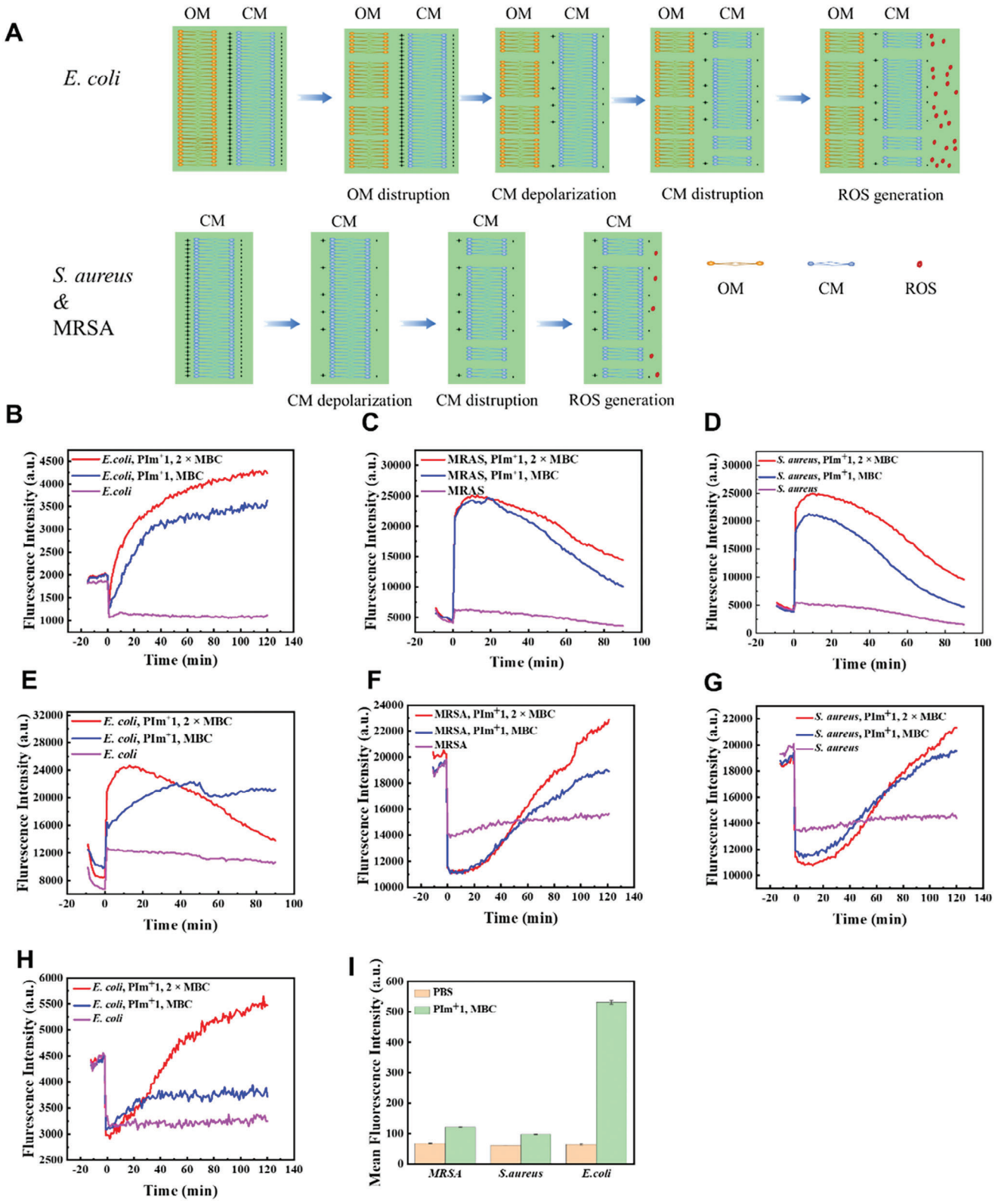

Figure 4. Membrane permeabilization and depolarization results of bacteria after being treated with PIm^+1. A) Schematic illustration of the action mechanisms of PIm^+ against *E. coli* and *S. aureus*. B) Outer membrane permeabilization assay for *E. coli* in the presence of PIm^+1 at MBC. Cytoplasmic membrane depolarization assay against C) MRSA, D) *S. aureus*, and E) *E. coli* at MBC and 2× MBC. Cytoplasmic membrane permeabilization assay against F) MRSA, G) *S. aureus*, and H) *E. coli* at MBC and 2× MBC. I) Intracellular ROS assay for MRSA, *S. aureus*, and *E. coli* at MBC in the presence of PIm^+1. The bacterial cells without polymers served as blank controls.

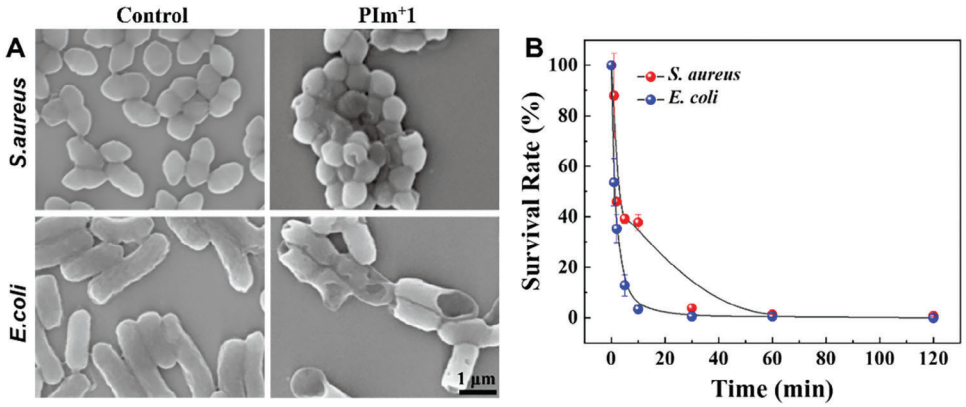

Figure 5. A) SEM images of *S. aureus* and *E. coli* before (control) and after treatment with PIm^+1. B) Bacterial killing kinetics of PIm^+1 against *S. aureus* and *E. coli* at MBC concentration. The scale bar represents a length of 1 μm.

achieving efficient sterilization of bacteria within biofilms necessitates the eradication of the biofilm structure itself. The eradication of biofilms presents a significant challenge due to the presence of densely packed EPS within the biofilm matrix. Consequently, an effective antibacterial polymer must not only possess the capacity to effectively kill bacteria but also disrupt the intricate biofilm matrix.

To assess the effectiveness of PIm^+1 in eradicating biofilms, biofilms of *S. aureus* and *E. coli* were cultured and subsequently treated with varying concentrations of PIm^+1 (ranging from 8 to 256 μg mL^{-1}) for 24 h. The remaining biofilm mass was then quantified to evaluate the biofilm eradication efficacy of PIm^+1. As illustrated in **Figure 6**A,B, the relative biofilm mass decreased with increasing concentrations of PIm^+1, indicating a concentration-dependent biofilm eradication behavior. Notably, the biofilm eradication process exhibited distinct differences between *S. aureus* and *E. coli*. Specifically, at a concentration of 16 μg mL^{-1} PIm^+1, 40% of the *S. aureus* biofilm was eradicated; while, only 30% of the *E. coli* biofilm was eradicated. However, at a concentration of 256 μg mL^{-1}, PIm^+1 demonstrated similar biofilm eradication efficiency for both strains, with ≈75–85% eradication observed after 24 h. However, as a positive control, Penicillin–Streptomycin showed less efficacy than PIm^+1 in eradicating bacterial biofilms at the concentration range of 16–256 μg mL^{-1} (Figure 6A,B; Figure S10, Supporting Information). It is important to mention that the concentration of 256 μg mL^{-1} corresponds to the HC_{10} value against RBC for PIm^+1 (Table 2), indicating its excellent biosafety when utilized for in vivo biofilm eradication purposes afterward.

Further, the process of biofilm permeabilization by PIm^+1 was visualized using confocal laser scanning microscopy (Figure S11, Supporting Information). Upon treatment of the biofilms with PIm^+1 for 120 min, a gradual increase in green emission intensity was observed, indicating the gradual penetration of PIm^+1 into the biofilm matrix and its interaction with bacteria within the biofilm. Following a 24-h incubation of *S. aureus* and *E. coli* biofilms with PIm^+1 at 2× MBC concentration, clear red emission from PI staining was observed in the CLSM images (Figure 6C). In contrast, the control samples (without PIm^+1 treatment) did not exhibit any red emission from PI staining. These results provide further evidence that PIm^+1 is capable of effectively eradicating bacterial biofilms; while, retaining its bactericidal activity.

3.4. Bacterial Resistance of PIm^+1

The emergence of bacterial resistance poses significant challenges to the effective application of antibiotics. Consequently, it is crucial to assess the potential for bacterial resistance development in PIm^+1 to evaluate its suitability as an antibacterial agent. In this study, *S. aureus* and *E. coli* were subjected to continuous exposure to PIm^+1 at a sublethal concentration (1/2× MIC) for 15 consecutive passages. The values of MIC_n/MIC_0 (where *n* represents the passage number) were determined for PIm^+1 against the cultured bacteria after each passage. Penicillin–Streptomycin was used as the positive control.

After subjecting *S. aureus* and *E. coli* to 15 cycles of exposure to PIm^+1, the values of MIC_n/MIC_0 remained constant at 1 and 2, respectively. In contrast, the values for the positive control significantly increased to 16 and 8, as depicted in **Figure 7**. These findings demonstrate that PIm^+1 does not promote the development of antibacterial resistance. This lack of resistance can be attributed to the membrane-disrupting mechanism of action exhibited by cationic antibacterial polymers, as opposed to inhibiting bacterial biosynthesis. Importantly, these results also highlight the considerable potential of PIm^+1 for application in the treatment of chronic bacterial infectious diseases.

4. Conclusion

A novel class of antibacterial polymers based on cationic imidazolium was synthesized successfully through 2 + 2 condensation polymerization of bi-imidazole and bi-chloride monomers. Systematic investigations revealed that the antibacterial performance, hemocompatibility, and biocompatibility of these polymers could be modulated by adjusting the hydrophobicity of the linkers connecting the two reactive sites. By carefully optimizing the lengths and types of linkers, a highly effective antibacterial polymer, PIm^+1, was synthesized. PIm^+1 exhibited remarkable bactericidal activity against various strains of bacteria and held

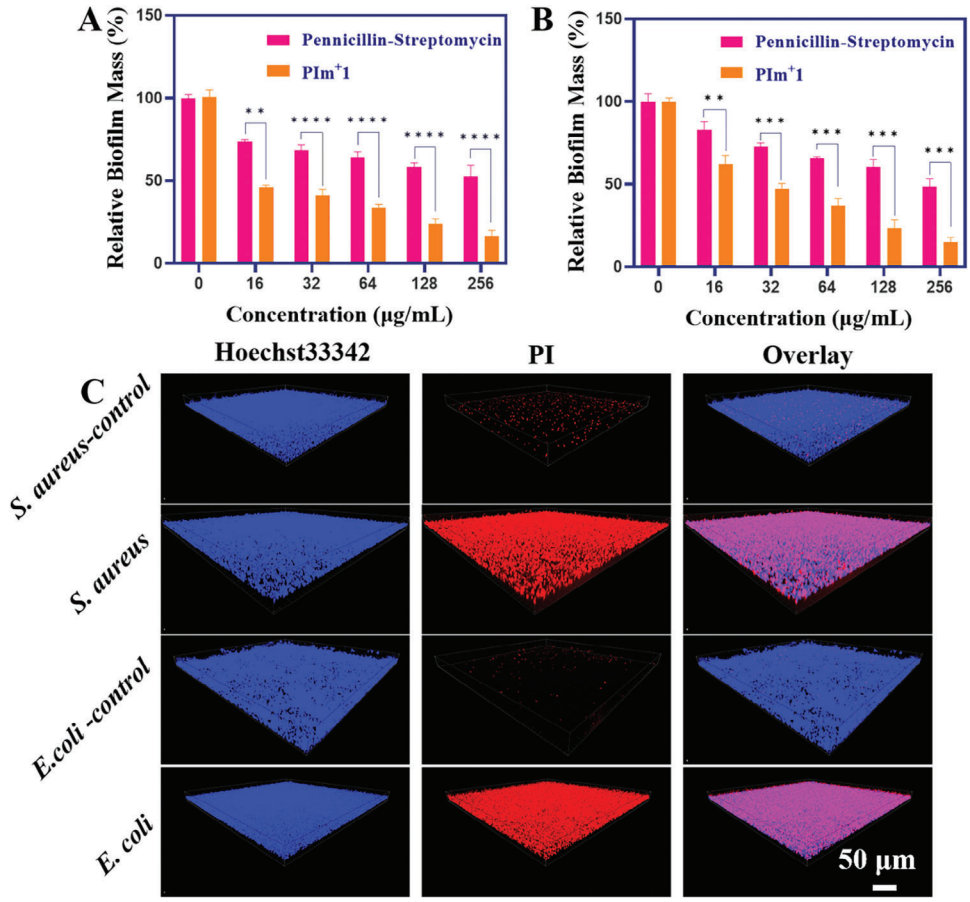

Figure 6. Biofilm eradication result of PIm$^+$1. A) The remaining biomass of the *S. aureus* biofilm after incubation with PIm$^+$1. B) The remaining biomass of the *E. coli* biofilm after incubation with PIm$^+$1. C) CLSM images of the *S. aureus* and *E. coli* biofilms, both untreated (control) and treated with PIm$^+$1 at MBC for 24 h. The scale bar represents a length of 50 μm.

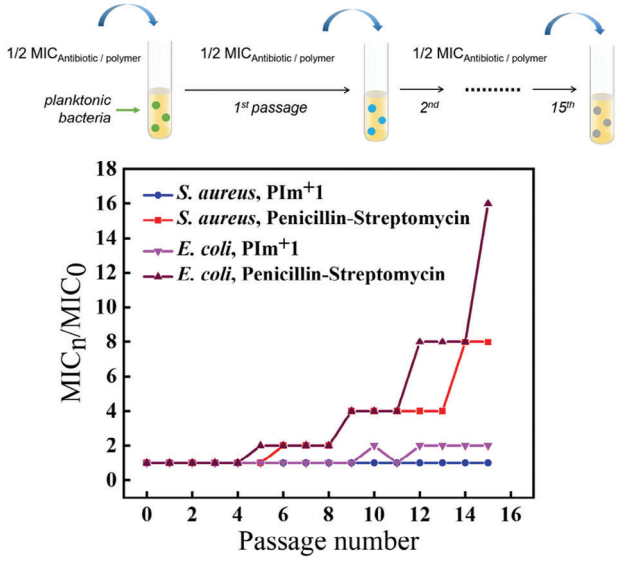

Figure 7. The results of bacterial resistance evaluation of PIm$^+$1 against *S. aureus* and *E. coli* after 15 cycles of passages.

excellent biosafety. Importantly, PIm$^+$1 not only displayed potent bactericidal and biofilm eradication capabilities but also exhibited negligible propensity for bacterial resistance against *S. aureus and E. coli*. These findings highlight the promising potential of PIm$^+$1 for the treatment of chronic wounds, and its application as antibacterial coatings for implantable medical devices.

Supporting Information

Supporting Information is available from the Wiley Online Library or from the author.

Acknowledgements

D.W. acknowledges the financial support of the National Natural Science Foundation of China (22075327) and of the Natural Science Foundation of Guangdong Province (2022A1515011392). R.W. acknowledges the financial support of the Shenzhen Municipal Scheme for Basic Research (JCYJ20210324100208022). S.C. acknowledges the Fundamental and Applied Research Foundation of Guangdong Province (2022A1515110441) and the Talent Research Project of the Shenzhen Natural Science Foundation (RCBS20221008093233049). In addition, Associate Prof. Jun Yue from the Sun Yat-Sen University is acknowledged for his constructive suggestion on antibacterial experiments.

Conflict of Interest

The authors declare no conflict of interest.

Data Availability Statement

The data that support the findings of this study are available from the corresponding author upon reasonable request.

Keywords

antibacterial polymers, antimicrobial agents, biofilms eradication, imidazolium

Received: October 27, 2023
Revised: December 14, 2023
Published online:

[1] A. Arora, A. Mishra, *Mater. Today: Proc.* **2018**, *5*, 17156.
[2] T. Li, Z. Wang, J. Guo, C. de. la Fuente-Nunez, J. Wang, B. Han, H. Tao, J. Liu, X. Wang, *Sci. Total Environ.* **2023**, *860*, 160461.
[3] K. V. R. Reddy, R. D. Yedery, C. Aranha, *Int. J. Antimicrob. Agents* **2004**, *24*, 536.
[4] R. M. Epand, H. J. Vogel, *Biochim. Biophys. Acta* **1999**, *1462*, 11.
[5] H. W. Huang, *Biochemistry* **2000**, *39*, 8347.
[6] M. Magana, M. Pushpanathan, A. L. Santos, L. Leanse, M. Fernandez, A. Ioannidis, M. A. Giulianotti, Y. Apidianakis, S. Bradfute, A. L. Ferguson, A. Cherkasov, M. N. Seleem, C. Pinilla, C. de. la. Fuente-Nunez, T. Lazaridis, T. Dai, R. A. Houghten, R. E. W. Hancock, G. P. Tegos, *Lancet Infect. Dis.* **2020**, *20*, e216.
[7] W. C. Wimley, K. Hristova, *J. Membr. Biol.* **2011**, *239*, 27.
[8] C. H. Chen, T. K. Lu, *Antibiotics* **2020**, *9*, 24.
[9] M. Mahlapuu, C. Björn, J. Ekblom, *Crit. Rev. Biotechnol.* **2020**, *40*, 978.
[10] K. Browne, S. Chakraborty, R. Chen, M. D. Willcox, D. S. Black, W. R. Walsh, N. Kumar, *Int. J. Mol. Sci.* **2020**, *21*, 7047.
[11] B. Bechinger, S.-U. Gorr, *J. Dent. Res.* **2017**, *96*, 254.
[12] S. Mankoci, J. Ewing, P. Dalai, N. Sahai, H. A. Barton, A. Joy, *Biomacromolecules* **2019**, *20*, 4096.
[13] C. Gong, J. Sun, Y. Xiao, X. Qu, M. Lang, *Adv. Healthcare Mater.* **2021**, *10*, 2101244.
[14] A. Som, S. Vemparala, I. Ivanov, G. N. Tew, *Pept. Sci.* **2008**, *90*, 83.
[15] M. Liu, L. Bauman, C. L. Nogueira, M. G. Aucoin, W. A. Anderson, B. Zhao, *Curr. Opin. Biomed. Eng.* **2022**, *22*, 100395.
[16] E.-R. Kenawy, S. D. Worley, R. Broughton, *Biomacromolecules* **2007**, *8*, 1359.
[17] S. Gupta, Y. M. Puttaiahgowda, A. Nagaraja, M. D. Jalageri, *Polym. Adv. Technol.* **2021**, *32*, 4642.
[18] M. S. Ganewatta, C. Tang, *Polymer* **2015**, *63*, A1.
[19] L. Timofeeva, N. Kleshcheva, *Appl. Microbiol. Biotechnol.* **2011**, *89*, 475.
[20] A. Jain, L. S. Duvvuri, S. Farah, N. Beyth, A. J. Domb, W. Khan, *Adv. Healthcare Mater.* **2014**, *3*, 1969.
[21] P. Pham, S. Oliver, C. Boyer, *Macromol. Chem. Phys.* **2023**, *22*, 2200226.
[22] Y. Luo, G. Yu, X. Liu, Y. Feng, P. Zhao, J. Yue, *Chem. Mater.* **2023**, *35*, 4705.
[23] E. M. Hetrick, M. H. Schoenfisch, *Chem. Soc. Rev.* **2006**, *35*, 780.
[24] J. Oh, A. Khan, *Biomacromolecules* **2021**, *22*, 3534.
[25] J. Sun, M. Li, M. Lin, B. Zhang, X. Chen, *Adv. Mater.* **2021**, *33*, 2104402.
[26] X. Wang, G. Wang, J. Zhao, Z. Zhu, J. Rao, *ACS Macro Lett.* **2021**, *10*, 1643.
[27] L. Bai, X. Tang, S. Kong, Y. Song, X. He, F. Meng, *Polym. Adv. Technol.* **2018**, *29*, 3106.
[28] Y. Xue, H. Xiao, Y. Zhang, *Int. J. Mol. Sci.* **2015**, *16*, 3626.
[29] A. Kanazawa, T. Ikeda, T. Endo, *J. Polym. Sci., Part A: Polym. Chem.* **1993**, *31*, 335.
[30] J. M. Antonucci, D. N. Zeiger, K. Tang, S. Lin-Gibson, B. O. Fowler, N. J. Lin, *Dent. Mater.* **2012**, *28*, 219.
[31] S. Imazato, S. Ma, J. Chen, H. H. K. Xu, *Dent. Mater.* **2014**, *30*, 97.
[32] Y. Ge, S. Wang, X. Zhou, H. Wang, H. H. K. Xu, L. Cheng, *Materials* **2015**, *8*, 3532.
[33] P. Makvandi, R. Jamaledin, M. Jabbari, N. Nikfarjam, A. Borzacchiello, *Dent. Mater.* **2018**, *34*, 851.
[34] J. Guo, J. Qin, Y. Ren, B. Wang, H. Cui, Y. Ding, H. Mao, F. Yan, *Polym. Chem.* **2018**, *9*, 4611.
[35] A. C. Engler, J. P. K. Tan, Z. Y. Ong, D. J. Coady, V. W. L. Ng, Y. Y. Yang, J. L. Hedrick, *Biomacromolecules* **2013**, *14*, 4331.
[36] F. Nederberg, Y. Zhang, J. P. K. Tan, K. Xu, H. Wang, C. Yang, S. Gao, X. D. Guo, K. Fukushima, L. Li, J. L. Hedrick, Y.-Y. Yang, *Nat. Chem.* **2011**, *3*, 409.
[37] W. Chin, C. Yang, V. W. L. Ng, Y. Huang, J. Cheng, Y. W. Tong, D. J. Coady, W. Fan, J. L. Hedrick, Y. Y. Yang, *Macromolecules* **2013**, *46*, 8797.
[38] C. Lin, Z. Ma, Y. Gao, M. Le, Z. Shi, D. Qi, J.-C. Ma, Z.-K. Cui, L. Wang, Y.-G. Jia, *ACS Appl. Mater. Interfaces* **2023**, *15*, 33444.
[39] P. R. Judzewitsch, T.-K. Nguyen, S. Shanmugam, E. H. H. Wong, C. Boyer, *Angew. Chem., Int. Ed.* **2018**, *57*, 4559.
[40] M. Porel, D. N. Thornlow, N. N. Phan, C. A. Alabi, *Nat. Chem.* **2016**, *8*, 590.
[41] S. Liu, R. J. Ono, H. Wu, J. Y. Teo, Z. C. Liang, K. Xu, M. Zhang, G. Zhong, J. P. K. Tan, M. Ng, C. Yang, J. Chan, Z. Ji, C. Bao, K. Kumar, S. Gao, A. Lee, M. Fevre, H. Dong, J. Y. Ying, L. Li, W. Fan, J. L. Hedrick, Y. Y. Yang, *Biomaterials* **2017**, *127*, 36.
[42] S. N. Riduan, Y. Yuan, F. Zhou, J. Leong, H. Su, Y. Zhang, *Small* **2016**, *12*, 1928.
[43] P. Li, C. Zhou, S. Rayatpisheh, K. Ye, Y. F. Poon, P. T. Hammond, H. Duan, M. B. Chan-Park, *Adv. Mater.* **2012**, *24*, 4130.
[44] E. F. Palermo, K. Lienkamp, E. R. Gillies, P. J. Ragogna, *Angew. Chem., Int. Ed.* **2019**, *58*, 3690.
[45] Y. Hu, J. Zhao, J. Zhang, Z. Zhu, J. Rao, *ACS Macro Lett.* **2021**, *10*, 990.
[46] J. W. Costerton, P. S. Stewart, E. P. Greenberg, *Science* **1999**, *284*, 1318.
[47] K. Sauer, P. Stoodley, D. M. Goeres, L. Hall-Stoodley, M. Burmølle, P. S. Stewart, T. Bjarnsholt, *Nat. Rev. Microbiol.* **2022**, *20*, 608.
[48] Y.-K. Wu, N.-C. Cheng, C.-M. Cheng, *Trends Biotechnol.* **2019**, *37*, 505.
[49] E. B. Anderson, T. E. Long, *Polymer* **2010**, *51*, 2447.
[50] A. Wang, S. Duan, Y. Hu, X. Ding, F.-J. Xu, *ACS Appl. Mater. Interfaces* **2022**, *14*, 44173.
[51] J.-R. Pouliot, F. Grenier, J. T. Blaskovits, S. Beaupré, M. Leclerc, *Chem. Rev.* **2016**, *116*, 14225.
[52] Y. Hu, J. Zhao, M. Yang, X. Wang, H. Zhang, J. Zhang, Z. Zhu, J. Rao, *ACS Appl. Polym. Mater.* **2022**, *4*, 4868.
[53] S. K. Sharma, G. S. Chauhan, R. Gupta, J.-H. Ahn, *J. Mater. Sci. Mater. Med.* **2010**, *21*, 717.
[54] C. Zhang, Y. Jiang, H. Ju, Y. Wang, T. Geng, *J. Mol. Liq.* **2017**, *241*, 638.
[55] N. Nikfarjam, M. Ghomi, T. Agarwal, M. Hassanpour, E. Sharifi, D. Khorsandi, M. Ali Khan, F. Rossi, A. Rossetti, E. Nazarzadeh Zare, N. Rabiee, D. Afshar, M. Vosough, T. Kumar Maiti, V. Mattoli, E. Lichtfouse, F. R. Tay, P. Makvandi, *Adv. Funct. Mater.* **2021**, *31*, 2104148.
[56] L. Carson, P. K. W. Chau, M. J. Earle, M. A. Gilea, B. F. Gilmore, S. P. Gorman, M. T. McCann, K. R. Seddon, *Green Chem.* **2009**, *11*, 492.